Final Report IREU 2023: Estimating Accuracy of Frequency Domain Models

Juan Granieri*

(Funded by the University of Florida, Gainesville
NSF Grant Number: NSF PHY-1950830)
(Dated: August 2023)

This project sought to compare the accuracy of gravitational wave waveform models generated in the frequency domain with models generated in the time domain. The accuracy would be determined by how well one model, called the template, would be able to recuperate an input signal parameter. This was done by first developing a set of tools which allowed for comparison between two waveforms. The frequency domain models were tested on themselves to see if these comparison methods were working, since the results are known. Interesting behavior was encountered here, and explored within the frequency domain models. After this, issues began to appear which made the comparison between the frequency domain generated waveforms and the time domain generated waveforms unfeasible.

I. INTRODUCTION

A. Gravitational Waves

Coming out of Einstein's theory of general relativity, gravitational radiation is emitted when the quadrupole moment of mass of a system has a non-zero second derivative in the transverse traceless (TT) gauge. The quadrupole moment of mass in the TT gauge is defined as

$$I_{ij} = \int\int\int \rho(s) S_{ij} d^3 s = \sum_p M_{(p)} S_{(p)ij} \tag{1}$$

where $\boldsymbol{s}$ is a position vector within the source/system, and S_{ij}, when we view the system from a location r where $r >> s$, is defined as

$$S_{ij} = s_i s_j - s_r(s_i n_j + s_j n_i) + \frac{1}{2} s_r^2 (n_i n_j + \delta_{ij}) + \frac{1}{2} s^2 (n_i n_j - \delta_{ij}) \tag{2}$$

where $\boldsymbol{n}$ is a unit vector in the $\boldsymbol{r}$ direction. Then, the instantaneous strain of the gravitational wave is given by

$$h_{ij}(t) = \frac{2G}{c^4 r} \ddot{I}_{ij}(t - r/c) \tag{3}$$

This gravitational wave strain is what travels through spacetime, and the spatial deformations these produce are what allows us to use interferometers to record data [2].

B. Background: Waveform Modelling

For the case of a binary system, such as the binary black hole systems which will be the only type analyzed in this paper, we are unable to predict exactly what the gravitational strain should look like given a certain set of system parameters. This is because there is no analytic solution to the two-body problem in GR. Thus, we are forced to make approximations and use numerical modelling to predict these.

Firstly, one can draw distinctions between different

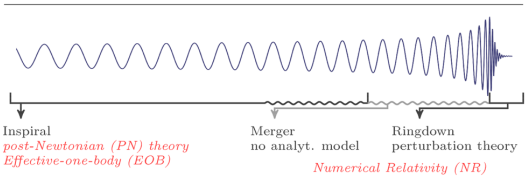

FIG. 1. Image from [5]. Here, we see a full time domain signal of gravitational wave strain vs. time. The different sections of the waveform are clearly labeled, and all of these must be modelled differently.

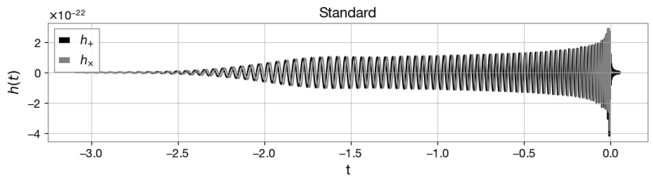

FIG. 2. An example of a time domain waveform generated using the lalsimulation package.

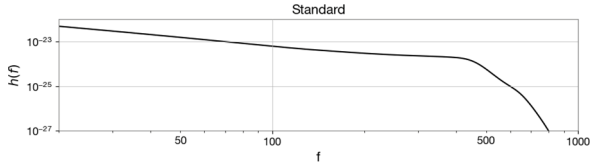

FIG. 3. An example of a frequency domain waveform generated using the lalsimulation package.

* University of Notre Dame, Class of 2024; jgranier@nd.edu

parts of the binary black hole (bbh) system's evolution, as can be seen in Figure 1. The inspiral represents the moments in the system where the black holes are far from each other and are orbiting at a fairly regular frequency. Since this, along with the fact that the velocity of the black holes in this region is far below the speed of light, allows for certain approximations to be made, we are able to model this region analytically. The merger represents the period in which the black holes get very near to each other and the speed of the black holes approaches that of light. In this region, the approximate solution to not describe the system well, and data from numerically solutions to the Einstein equation is used to help inform this part of the evolution. The ringdown represents the point in which the black holes have finally made contact with each other and are merging into one black hole. Here, the velocities are very near that of light and the gravitational field is very strong, making all of the low-relativistic assumptions nonsensical. Here, only the numerical solutions of the Einstein equations are able to provide accurate information.

There are various different models out which create the waveforms for bbh systems. Among them is the Effective One Body (EOBNR) family, which reduce the bbh problem to a one body problem, and then solve the system of equations for this problem in order to model the behavior of the bbh system. This model uses post-Newtonian approximants to model the system and then merges the results to those of numerical relativity data. Important to note for this project, these waveforms are generated in the time domain. The NRSurrogate waveforms are generated by numerically solving the Einstein equations for the bbh system, which makes this method the most accurate out of all of these options. This method is also very computationally expensive. However, NRSurrogate is only able to be used in certain regions of the parameter space (for high masses, for example) which restricts its ability to be used. These waveforms are also generated in the time domain. This method is also computationally expensive. The Phenomenological (Phenom) family is yet another method, which makes use of of post-Newtonian approximants (like the EOB models), but creates the waveforms in the frequency domain. These waveforms are then merged to the numerical relativity data for the merger and ringdown.

The models all make use of a set of source parameters, such as the mass ratio between the two black holes (defined as the ratio of the lower mass black hole in the system to that of the higher), the total mass of the system, and the spin of each black hole (in all three spatial directions). The coordinate system for binary black hole systems is set such that the two black holes orbit each other entirely in the x-y plane. Also useful to note is the chirp mass, which is a combination of mass and mass ratio which is measured by the detectors. Chirp mass is defined as

$$M_c = \frac{Mq^{3/5}}{(1+q)^{6/5}} \tag{4}$$

where M is the total mass of the bbh system and q the mass ratio described just now [5].

II. MATH

In order to compare waveform models, we must describe a set of mathematical tools which allow us to do to do this. Let us define θ as the source parameters used to generate the waveform. Then $h(\theta)$ is one waveform generated with the source parameters, and $h(\theta_0)$ is another signal generated using a different set of parameter values. Then we define the inner product between two different waveform signals as

$$\langle h(\theta)|h(\theta_0)\rangle = 4Re\int_{f_{min}}^{f_{max}} \frac{\tilde{h}(\theta)\tilde{h_2}^*(\theta_0)}{S_n(f)}df \tag{5}$$

where $S_n(f)$ is the instrument's noise spectral density and $\tilde{h}$ represents h in the Fourier domain [6].
Using this definition, we are able to define a quantity referred to as the overlap which is representative of the "overlap" between the two normalized gravitational wave signals.

$$\mathcal{O} = \left\langle \hat{h}(\theta)\middle|\hat{h}(\theta_0)\right\rangle = \frac{\langle h(\theta)|h\theta_0\rangle}{\langle h(\theta)|h(\theta)\rangle\,\langle h(\theta_0)|h(\theta_0)\rangle} \tag{6}$$

This is a kind of extension of the inner product as used for vectors, where instead of vectors we are using the waveform signals [3]. Note that the hatted signals denote the normalized signals.
We must also define a parameter Λ called the likelihood defined as

$$\Lambda = \frac{exp(-\langle h(\theta_0)-h(\theta)|h(\theta_0)-h(\theta)\rangle/2)}{exp(-\langle h(\theta_0)|h(\theta_0)\rangle/2)} \tag{7}$$

[6]. Here, we must also introduce the concept of marginalization, or optimization. When we do not know the value of a certain parameter, or want to take into account that it could fall within a range of values, we are able to do this by integrating the parameter out of the posterior probability. Thus, no information is lost since we are including all we know, and yet it allows us to create a more restrained estimate for our posterior likelihood values. While this tangent is a bit out of place within this paper, and the details lie outside of the scope what this project sought to accomplish, this mention is important since optimization played a vital role within this project. To add a concrete example, one optimization done was phase optimization. Since the bbh system's starting phase has nothing to do with the systems evolution (i.e. the initial phase has only to do with the orientation of the chosen coordinate system) marginalization over this parameter erases all effects the initial phase might have on the signal. This allow us to compare two waveforms 'apples-to-apples' since all non-physical effects have been erased. A similar process can be done for time optimization [4].

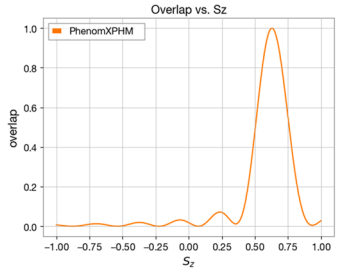

FIG. 4. Overlap value vs. spin in z direction plot for IMRPhenomXPHM model compared to self. The signal has a total spin in the z direction of 0.66. Here, we see how the overlap value varies along the parameter space, and we can see how well the model is able to recover the value of the parameter based on where the overlap value peaks.

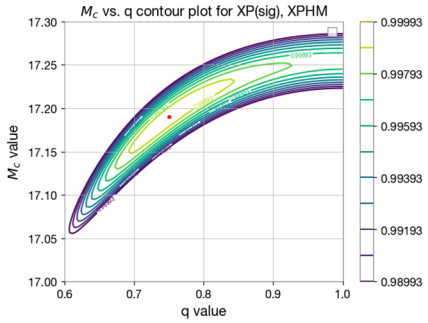

FIG. 5. Overlap values over a section of the chirp mass-mass ratio parameter space for a IMRPhenomXP generated signal with an IMRPhenomXPHM template. In red is the true signal value, and some of the contours of the overlap values between the signal and the template are shown.

We then define the phase optimized log-likelihood as

$$\max_{\|h(\theta)\|} log(\Lambda) = -\frac{1}{2}\|h(\theta_0)\|^2(1 - \left\langle \hat{h}(\theta_0)\middle|\hat{h}(\theta)\right\rangle^2) \quad (8)$$

This likelihood is important to us since it scales with the posterior probability, but which we will not go into as this goes outside of the scope of this project [1].

III. METHODS

This project made use of the frequency domain Phenomenological models to generate the waveforms. This was done via the lalsimulation python package which allows one to generate waveforms.

As we can see in Figures 2 and 3, the simulation generates a signal spanning a desired time or frequency length. Once generated, these signals can then be subjected to analysis via the tools defined in Section II. Within the scope of this project, the overlap was the main method of quantifying how different two waveform models were.

Since the project sought to measure the accuracy of the frequency domain waveform models, this was done by seeing how well one model was able to 'recover' another. To do this, a signal waveform is first generated using one of the generating models and a series of template waveforms are also generated. The templates waveforms can be generated using the same waveform model, or using another. Now, using the template models, which are generated at various points throughout the parameter space, we can calculate the overlap that these templates have with the signal. By doing this we can see how well the template is able to recover the original signal, i.e., at the point of maximum overlap between the two waveforms being compared, how close are the parameters of the template to the parameters of the signal. Thus, we are able to see how accurately the template is able to replicate the signal within a certain part of the parameter space.

As we can see in Figure 4, when a waveform generation model is compared to itself along the parameter space, it is able to recover very accurately, since the overlap plot peaks when the template parameter value is equal to the parameter value of the signal. Part of how accurately this is able to be done has to do with the density of the grid used, but for the scope of this project grids were made dense enough so that taking less or more points made very little difference to the shape of the plot and did not lead to much better results. For the 1-dimensional plots, this was taken to be anything greater than 101 steps, and for two dimensional plots a 101x101 mesh. An example of one of these two-dimensional overlap plots can be found in Figure 5.

Using the method shown in 4, one can compare different waveform models against each other to see how well one is able to recover the values of the other. This project sought to see how well frequency domain models were able to recover the parameters of signals generated using time domain models. Thus, this method of calculating the overlap between two different waveforms over the parameter space proves useful for measuring the accuracy of one waveform in picking up the parameter values of another.

In order to ensure that the density of the parameter space grid does not influence how accurate the recuperated parameters, an optimizing function was also created. This function takes the signal waveform and the template generator, and then employs a minimization scheme across a desired region of the parameter space. This allows the function to find the values for the template parameters which maximizes the overlap between the two. In Figure 5, the input signal had a chirp mass of 17.19 solar masses and a mass ratio of 0.75. The ideal parameter values for the template, found sing the optimizer, recovered a chirp mass of 17.189 and a mass ratio of 0.749, demonstrating that in this particular case the template is able to recover the signal to a great degree of accuracy. Since both of these waveform models come from the same family, however, all this demonstrates is

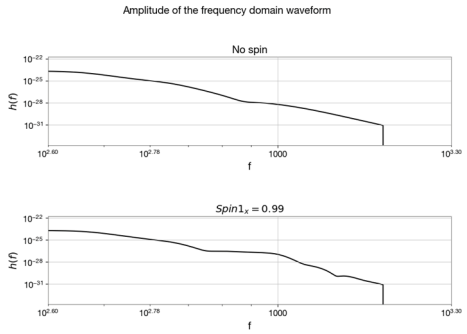

FIG. 6. Frequency domain plot showing the strain value vs. frequency for two models generated using IMRPhenomXPHM. The only difference between the two waveforms lies in their spin values. Notice the strange 'rigid' behavior displayed by the curve when precession (spin in x or y direction) is introduced.

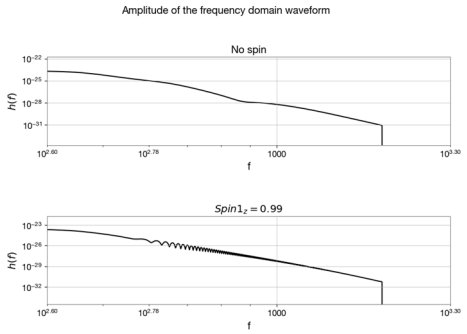

FIG. 7. Frequency domain plot showing the strain value vs. frequency for two models generated using IMRPhenomXPHM. The only difference between the two waveforms lies in their spin values. Notice the oscillating strain for frequencies over 200 Hz.

that this optimizing function is in working order and can be applied with reasonable certainty to cases in which the waveforms are generated via different model families.

IV. ANALYSIS

A. Initial Findings

Within the entirety of this experiment, it was assumed that the signal to noise ratio, S_n, was equal to 1. Taking a look at Section III, we can see that this value is involved as scaling of the values at different frequencies. Since this project sought to see how the models behaved at a basic level, this simplification was added so that all effects would be due entirely to differences within the waveform models themselves. To add a non-unity signal to noise ratio would have added another layer of complexity outside of the basic scope of what this project was seeking to accomplish.

The analysis began with first confirming that the waveform generators were up and functioning (the Python interface for this seems to be new, and thus the possibility of bugs and such loomed large). After generating some simple plots, see Figures 2 and 3, the rest of the parameter space began to be explored to see if there any unexpected behaviors which began to appear.

The most interesting of such unexpected behavior appeared in the frequency domain strain plots when a high spin was added to the system, as in Figures 6 and 7. In the frequency ranges above 200 Hz or so, both plots seem to display some sort of strange oscillations in the strain, which does not have any physical reason for showing up here, given that the only thing that is being changed in the system is the spin of the black holes. In order to investigate this further, a frequency to time mapping was created in order to see if these effects could be located to certain time regions in the black hole's orbits.

This mapping can be seen in Figure 8 for a relatively

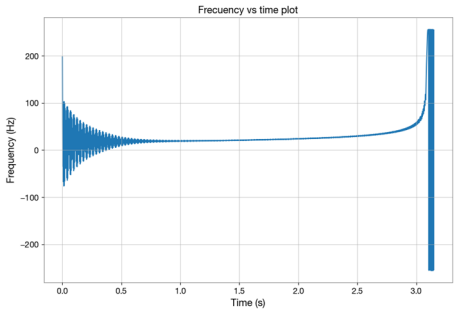

FIG. 8. Time to frequency mapping (also known as chirp plot) for a waveform without spin.

normal waveform (no spin or extreme parameters). Towards the end of the figure however, we know that the merger must take place in the last bit of the waveform, and we can recognize this as the section of the plot in which the frequency begins displaying bizarre behavior by oscillating wildly. Since this behavior can be regarded as nonphysical, we remove the merger from our mapping analysis and limit our mapping to the region without the merger, as shown in Figure 9. Thus, we have our mapping and can see which times frequencies correspond to

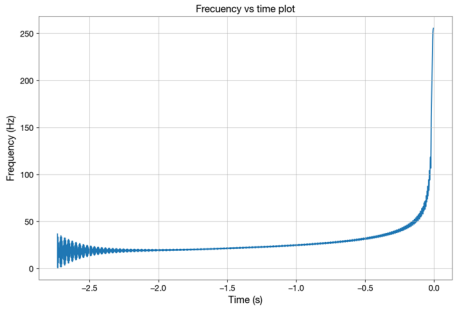

FIG. 9. Figure 8 with the merger taken out of the mapping on the grounds that it is unphysical.

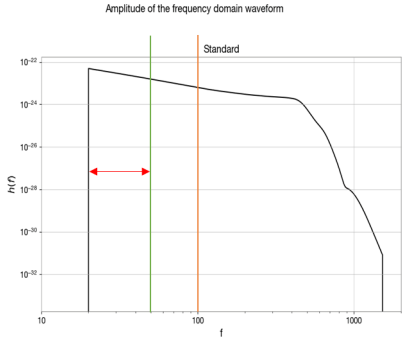

FIG. 10. Here we see the frequency domain waveform with limits added in. The vertical orange line, located at 100 Hz (150 Hz before the cutoff in Figure 9), shows how the strange behavior for this system takes place well after the 100 Hz mark.

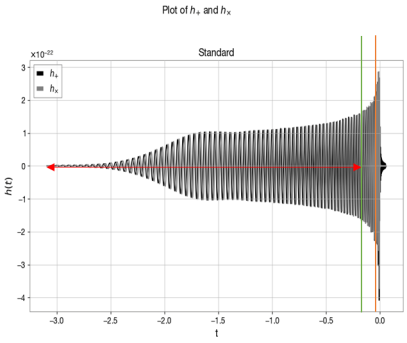

FIG. 11. Here we can see, using the time-frequency mapping, where the limits from Figure 10 land on the time domain. We notice that the 100 Hz marker takes place almost at the very end of the waveform, well into the merger. Since the merger is where the model breaks down a bit, it is perfectly acceptable for a bit of non-physical behavior to be appearing in this range, showing that there is no serious issue here with the model.

which times, with the small hiccup at the beginning of the plot being a limitation of the model's not being able to generate waveforms that come from infinitely far away.

With this mapping, we can see that many of the strange effects in the frequency domain take place after the merger 'cutoff point' of around 250 Hz. Looking at Figures 10 and 11, we can see that almost all of the strange behavior that takes place occurs after the vertical orange line in both of these plots. Thus, we see that the strange variations in the strain take place almost entirely within the last 10th of a second of the signal. This region is well within the merger, where the models break down, and so it was found that this behavior was nothing with which one ought to be concerned with.

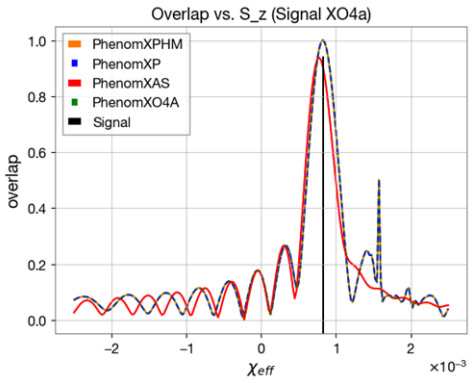

FIG. 12. Here we see the signal-template overlap values for different values of χ_{eff} (a parameter related to the total spin of the system). In this case, the signal, denoted by the black vertical line, is located at the χ_{eff} value corresponding to both black holes in the bbh system having a spin of 0.33. We see that the newer models are able to recover the parameter almost exactly, but that a strange secondary peak seems to form to the right of this.

B. Spin Behavior

After these initial forays into waveform generating and studying the basic behavior of the waveforms, the project moved more towards exploring how the waveforms changed along the parameter space. Much of the behavior encountered was expected, like a time domain waveform decreasing in length when the black holes are more massive (resulting in less of an inspiral and thus less of a signal), but some of the behavior seemed to have no physical explanation.

This strange non-physical behavior was one of the things the project was particularly interested in, since these features could possibly be due to limitations of the models. The most interesting of the observed behaviors came from varying the value of the spin in the z direction of one or both of the black holes in the binary system. This behavior consisted of a consistent peak in the template-signal overlap values at the point at which the black hole(s) with spin in the system had a z direction spin value of 0.66. This behavior took place no matter the spin value the black hole(s) had in the signal case, although the effect became more dramatic the closer one got to this troublesome point.

As can be seen in Figure 12, there is a peak of the overlap value for the case in which both (in this case) black holes in the system have a spin of 0.66. Notice, however, that this takes place for the IMRPhenom XPHM, XP, and XO4a models and not for XAS. However, XAS does not recuperate the signal spin value as well as the other models. This is because XAS is an older member of the phenom family, meaning that this unexplained peak is a result of one of the changes made in the models between the XAS and XP models. While the details of this are much too technical and not very related to the main goal

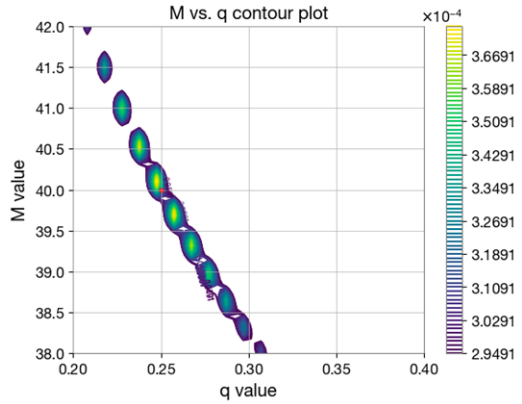

FIG. 13. Here we see a total mass vs. mass ratio (q) plot without time optimization. As opposed to Figure 5, this signal point is located at a much smaller value in the mass ratio space. In this region, a strange kind of 'beading' behavior began to be observed as can be seen in the figure, which made no physical sense.

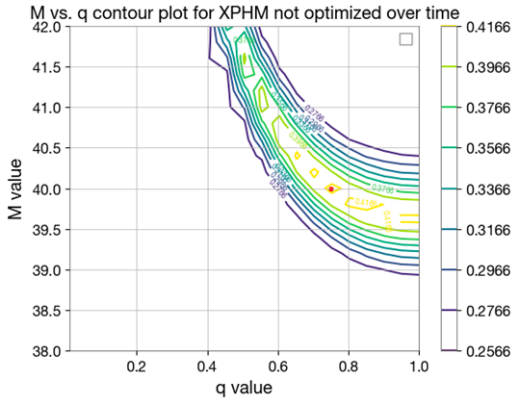

FIG. 14. Here we see a total mass vs. mass ratio (q) plot where the time optimization was not implemented. Notice how the contours have jagged edges, and how there is a lot of 'beading' occurring throughout the plot, most notably in the inner contours.

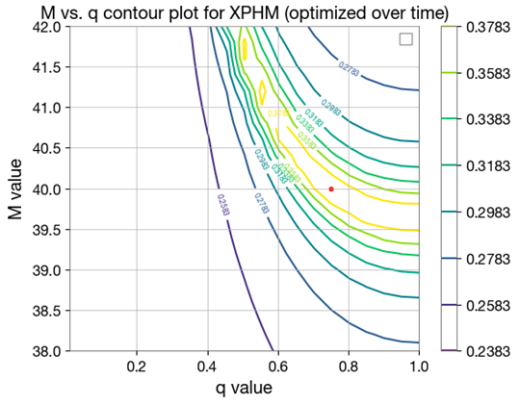

FIG. 15. Here we see a total mass vs. mass ratio (q) plot where the time optimization was implemented. Notice that compared to Figure 14, there is much more smoothing in the inner contour. However, the 'beading' still occurs and the contours continue to have non-smooth boundaries, showing that the optimization over time was still not functioning correctly.

of the experiment, the investigation was stopped here. However, conversation with one of the Postdocs involved in my project, Shrobana Ghosh, led to a speculation that this peak might be due to how spins are handled in the newer models which take precession into account (i.e., all the models here besides XAS).

C. Updating Functions,

After this parameter behavior was observed, the project became a bit more focused on the contour plots (see Figure 5). It was noticed that, while the contour plots were very good in certain regions of the chirp mass-mass ratio parameter space, there were other regions in which the contour seemed to fail rather miserably. As one can see in Figure 13, the contour began displaying some sort of strange 'beading' behavior in which certain regions of the parameter space achieved greater signal-template overlap values than others, despite the fact that the contours should, even if peaking in another region, display a 'normal' behavior in which the contours form consistently around a clear maximum. In this case, and others, there appears to be no maximum, but just a series of regions in which the template appears to recover the signal to the same extent, despite these regions varying greatly over the space.

Since this kind of behavior should not be taking place, it was thought that perhaps this 'beading' could be due to the fact that the overlap values had thus far only been phase optimized and not time optimized (see section III). So, a time optimized overlap function was created and implemented.

Looking at Figures 14 and 15, we can see that much of the beading, especially in the inner contour, is smoothed out by the time optimization. However, beading still appears and the contour lines have some 'wavy' behavior which was not expected. After many laborious weeks of trying to fix this time optimization, issues persisted and no fully successful time optimization was ever developed. The main issue was with an inverse Fourier transform which one must do in order to take the frequency domain waveform to the time domain to undertake the optimization process.

D. Final Results (or lack thereof)

After this exploration of the Phenomenological models, the idea was to move towards comparing the performance of the frequency domain Phenomenological mod-

els to that of the time domain SEOBNR models. When the project had finally advanced to the point that this step could be reached however, it was realized the the EOB waveform model family was not working on the lalsimulation interface being used for this project. Many at temps were made to try to get the EOB waveforms to generate on Python by downloaded various packages and sending emails to the code's developers. Problems with the code, a lack of time on the part of the developers, and the drawing near of the deadline date for this project made this comparison impossible, and so an alternative had to be looked for.

Thus, the project shifted from a comparison with the EOB waveform family to one with the NRSurrogate family. These waveform models were able to be generated, with great difficulty. However, when it came time to come up with a comparison between the frequency domain and time domain models, the inverse Fourier transform and the Fourier transform (used on the time domain NRSurrogate waveform to bring it to frequency domain) created issues and led to many difficulties which this project was unable to resolve. Among the difficulties encountered were learning how the inverse Fourier transform works on Python, since this requires inputs to have a specific notation. Then, issues with the spacing of the frequency binning on the Fourier transformed waveform made so that the waveforms could not be compared, since the waveforms being compared using the overlap function must be of the same length and need to cover the same amount of the frequency space. Some partial solutions were found, but these error compounded with the still unfixed troubles of the the inverse Fourier transform discussed in Section IV C to create a disaster. Some overlap contour plots were able to be created between a time domain generated (NRSurrogate) signal and a frequency domain (Phenom) generated template. However, given that the time optimization was still nonfunctional and that the methods by which the comparison was made possible (through using interpolations and 'forcing' the frequency binning to match) made such a comparison practically meaningless, and so the plots are not included within this report.

V. CONCLUSION

In conclusion, the project failed in reaching its goal of comparing the frequency domain generated Phenom models with the time domain generated EOB or NRSurrogate models. While technical difficulties outside of the project's control prevented the first of these comparisons, the second comparison was attempted but uncompleted due to issues encountered with the Fourier/inverse Fourier transform.

VI. FUTURE WORK

Any continuation of this work would firstly involve a fixing of the inverse Fourier transform. Conversations with colleagues have led to some suggestions which merit trying, such as applying windowing functions, applying smoothing functions after taking the transform, and playing around with the time domain binning so that the frequency space binning does not need to be tampered with after the transform. All of this also entails a deeper understanding of how the numpy fft library operates, which would require investigation in its own right. Ensuring that the time optimization works would be the first and foremost continuation. The optimizer function would also have to be updated for this analysis, since it was not functioning whenever the time domain waveform was compared to the frequency domain waveform. This could very well have been due to the approximate way in which this analysis was 'forced' into happening, but this would have to be checked before one could proceed into a detailed comparison of the two waveforms.

After this, colleagues have also suggested making the comparison between the two models in the time domain. Since the time domain is a bit more intuitive to work with physically, it might be better to do the analysis in this way at first so that one can make sure that taking the frequency domain generated waveforms to the time domain works smoothly. Then, if desired, the opposite of this could be done to the time domain generated model and the analysis could be continued as was planned originally. By this point, the frequency binning issues would have been resolved and a comparison which is both accurate and straightforward should be able to be done. Finally, and most obviously, it would be very interesting to make a comparison with the EOB waveforms as was the initial intention of the project. This would of course depend on the appropriate code being released, and in this sense remains out of the author's control, yet there is reason to believe that this take place soon and thus could be included in a potential follow up.

VII. ACKNOWLEDGEMENTS

Special thanks to my mentor, Dr. Frank Ohme, and his group, Dr. Shrobana Ghosh, Angela Borchers Pascual, Dr. Wolfgang Kastaun, Jannik Mielke, and Robert Halbach, for all of their guidance, friendliness, and a great summer experience.

VIII. REFERENCES

[1] B P Abbott, R Abbott, T D Abbott, S Abraham, F Acernese, K Ackley, C Adams, V B Adya, C Affeldt, M Agathos, K Agatsuma, N Aggarwal, O D Aguiar,

L Aiello, A Ain, P Ajith, T Alford, G Allen, A Allocca, M A Aloy, P A Altin, A Amato, A Ananyeva, S B Anderson, W G Anderson, S V Angelova, S Antier, S Appert, K Arai, M C Araya, J S Areeda, M Arène, N Arnaud, K G Arun, S Ascenzi, G Ashton, S M Aston, P Astone, F Aubin, P Aufmuth, K AultONeal, C Austin, V Avendano, A Avila-Alvarez, S Babak, P Bacon, F Badaracco, M K M Bader, S Bae, P T Baker, F Baldaccini, G Ballardin, S W Ballmer, S Banagiri, J C Barayoga, S E Barclay, B C Barish, D Barker, K Barkett, S Barnum, F Barone, B Barr, L Barsotti, M Barsuglia, D Barta, J Bartlett, I Bartos, R Bassiri, A Basti, M Bawaj, J C Bayley, M Bazzan, B Bécsy, M Bejger, I Belahcene, A S Bell, D Beniwal, B K Berger, G Bergmann, S Bernuzzi, J J Bero, C P L Berry, D Bersanetti, A Bertolini, J Betzwieser, R Bhandare, J Bidler, I A Bilenko, S A Bilgili, G Billingsley, J Birch, R Birney, O Birnholtz, S Biscans, S Biscoveanu, A Bisht, M Bitossi, M A Bizouard, J K Blackburn, C D Blair, D G Blair, R M Blair, S Bloemen, N Bode, M Boer, Y Boetzel, G Bogaert, F Bondu, E Bonilla, R Bonnand, P Booker, B A Boom, C D Booth, R Bork, V Boschi, S Bose, K Bossie, V Bossilkov, J Bosveld, Y Bouffanais, A Bozzi, C Bradaschia, P R Brady, A Bramley, M Branchesi, J E Brau, T Briant, J H Briggs, F Brighenti, A Brillet, M Brinkmann, V Brisson, P Brockill, A F Brooks, D D Brown, S Brunett, A Buikema, T Bulik, H J Bulten, A Buonanno, D Buskulic, C Buy, R L Byer, M Cabero, L Cadonati, G Cagnoli, C Cahillane, J Calderón Bustillo, T A Callister, E Calloni, J B Camp, W A Campbell, M Canepa, K C Cannon, H Cao, J Cao, E Capocasa, F Carbognani, S Caride, M F Carney, G Carullo, J Casanueva Diaz, C Casentini, S Caudill, M Cavaglià, F Cavalier, R Cavalieri, G Cella, P Cerdá-Durán, G Cerretani, E Cesarini, O Chaibi, K Chakravarti, S J Chamberlin, M Chan, S Chao, P Charlton, E A Chase, E Chassande-Mottin, D Chatterjee, M Chaturvedi, K Chatziioannou, B D Cheeseboro, H Y Chen, X Chen, Y Chen, H-P Cheng, C K Cheong, H Y Chia, A Chincarini, A Chiummo, G Cho, H S Cho, M Cho, N Christensen, Q Chu, S Chua, K W Chung, S Chung, G Ciani, A A Ciobanu, R Ciolfi, F Cipriano, A Cirone, F Clara, J A Clark, P Clearwater, F Cleva, C Cocchieri, E Coccia, P-F Cohadon, D Cohen, R Colgan, M Colleoni, C G Collette, C Collins, L R Cominsky, M Constancio, L Conti, S J Cooper, P Corban, T R Corbitt, I Cordero-Carrión, K R Corley, N Cornish, A Corsi, S Cortese, C A Costa, R Cotesta, M W Coughlin, S B Coughlin, J-P Coulon, S T Countryman, P Couvares, P B Covas, E E Cowan, D M Coward, M J Cowart, D C Coyne, R Coyne, J D E Creighton, T D Creighton, J Cripe, M Croquette, S G Crowder, T J Cullen, A Cumming, L Cunningham, E Cuoco, T Dal Canton, G Dálya, S L Danilishin, S D'Antonio, K Danzmann, A Dasgupta, C F Da Silva Costa, L E H Datrier, V Dattilo, I Dave, M Davier, D Davis, E J Daw, D DeBra, M Deenadayalan, J Degallaix, M De Laurentis, S Deléglise, W Del Pozzo, L M DeMarchi, N Demos, T Dent, R De Pietri, J Derby, R De Rosa, C De Rossi, R DeSalvo, O De Varona, S Dhurandhar, M C Díaz, T Dietrich, L Di Fiore, M Di Giovanni, T Di Girolamo, A Di Lieto, B Ding, S Di Pace, I Di Palma, F Di Renzo, A Dmitriev, Z Doctor, F Donovan, K L Dooley, S Doravari, I Dorrington, T P Downes, M Drago, J C Driggers, Z Du, J-G Ducoin, P Dupej, S E Dwyer, P J Easter, T B Edo, M C Edwards, A Effler, P Ehrens, J Eichholz, S S Eikenberry, M Eisenmann, R A Eisenstein, R C Essick, H Estelles, D Estevez, Z B Etienne, T Etzel, M Evans, T M Evans, V Fafone, H Fair, S Fairhurst, X Fan, S Farinon, B Farr, W M Farr, E J Fauchon-Jones, M Favata, M Fays, M Fazio, C Fee, J Feicht, M M Fejer, F Feng, A Fernandez-Galiana, I Ferrante, E C Ferreira, T A Ferreira, F Ferrini, F Fidecaro, I Fiori, D Fiorucci, M Fishbach, R P Fisher, J M Fishner, M Fitz-Axen, R Flaminio, M Fletcher, E Flynn, H Fong, J A Font, P W F Forsyth, J-D Fournier, S Frasca, F Frasconi, Z Frei, A Freise, R Frey, V Frey, P Fritschel, V V Frolov, P Fulda, M Fyffe, H A Gabbard, B U Gadre, S M Gaebel, J R Gair, L Gammaitoni, M R Ganija, S G Gaonkar, A Garcia, C García-Quirós, F Garufi, B Gateley, S Gaudio, G Gaur, V Gayathri, G Gemme, E Genin, A Gennai, D George, J George, L Gergely, V Germain, S Ghonge, Abhirup Ghosh, Archisman Ghosh, S Ghosh, B Giacomazzo, J A Giaime, K D Giardina, A Giazotto, K Gill, G Giordano, L Glover, P Godwin, E Goetz, R Goetz, B Goncharov, G González, J M Gonzalez Castro, A Gopakumar, M L Gorodetsky, S E Gossan, M Gosselin, R Gouaty, A Grado, C Graef, M Granata, A Grant, S Gras, P Grassia, C Gray, R Gray, G Greco, A C Green, R Green, E M Gretarsson, P Groot, H Grote, S Grunewald, P Gruning, G M Guidi, H K Gulati, Y Guo, A Gupta, M K Gupta, E K Gustafson, R Gustafson, L Haegel, O Halim, B R Hall, E D Hall, E Z Hamilton, G Hammond, M Haney, M M Hanke, J Hanks, C Hanna, M D Hannam, O A Hannuksela, J Hanson, T Hardwick, K Haris, J Harms, G M Harry, I W Harry, C-J Haster, K Haughian, F J Hayes, J Healy, A Heidmann, M C Heintze, H Heitmann, P Hello, G Hemming, M Hendry, I S Heng, J Hennig, A W Heptonstall, Francisco Hernandez Vivanco, M Heurs, S Hild, T Hinderer, D Hoak, S Hochheim, D Hofman, A M Holgado, N A Holland, K Holt, D E Holz, P Hopkins, C Horst, J Hough, E J Howell, C G Hoy, A Hreibi, E A Huerta, D Huet, B Hughey, M Hulko, S Husa, S H Huttner, T Huynh-Dinh, B Idzkowski, A Iess, C Ingram, R Inta, G Intini, B Irwin, H N Isa, J-M Isac, M Isi, B R Iyer, K Izumi, T Jacqmin, S J Jadhav, K Jani, N N Janthalur, P Jaranowski, A C Jenkins, J Jiang, D S Johnson, A W Jones, D I Jones, R Jones, R J G Jonker, L Ju, J Junker, C V Kalaghatgi, V Kalogera, B Kamai, S Kandhasamy, G Kang, J B Kanner, S J Kapadia, S Karki, K S Karvinen, R Kashyap, M Kasprzack, S Katsanevas, E Katsavounidis, W Katzman, S Kaufer, K Kawabe, N V Keerthana, F Kéfélian, D Keitel, R Kennedy, J S Key, F Y Khalili, H Khan, I Khan, S Khan, Z Khan, E A Khazanov, M Khursheed, N Kijbunchoo, A X Kim, Chunglee Kim, J C Kim, K Kim, W Kim, W S Kim, Y-M Kim, C Kimball, E J King, P J King, M Kinley-Hanlon, R Kirchhoff, J S Kissel, L Kleybolte, J H Klika, S Klimenko, T D Knowles, P Koch, S M Koehlenbeck, G Koekoek, S Koley, V Kondrashov, A Kontos, N Koper, M Korobko, W Z Korth, I Kowalska, D B Kozak, V Kringel, N Krishnendu, A Królak, G Kuehn, A Kumar, P Kumar, R Kumar, S Kumar, L Kuo, A Kutynia, S Kwang, B D Lackey, K H Lai, T L Lam, M Landry, B B Lane, R N Lang, J Lange, B Lantz, R K Lanza, S Larson, A Lartaux-Vollard, P D Lasky, M Laxen, A Lazzarini, C Lazzaro, P Leaci, S Leavey, Y K Lecoeuche, C H Lee, H K Lee, H M Lee, H W Lee, J Lee, K Lee, J Lehmann, A Lenon, N Leroy, N Letendre, Y Levin, J Li, K J L Li, T G F Li, X Li, F Lin, F Linde, S D Linker, T B Lit-

tenberg, J Liu, X Liu, R K L Lo, N A Lockerbie, L T London, A Longo, M Lorenzini, V Loriette, M Lormand, G Losurdo, J D Lough, C O Lousto, G Lovelace, M E Lower, H Lück, D Lumaca, A P Lundgren, R Lynch, Y Ma, R Macas, S Macfoy, M MacInnis, D M Macleod, A Macquet, F Magaña-Sandoval, L Magaña Zertuche, R M Magee, E Majorana, I Maksimovic, A Malik, N Man, V Mandic, V Mangano, G L Mansell, M Manske, M Mantovani, F Marchesoni, F Marion, S Márka, Z Márka, C Markakis, A S Markosyan, A Markowitz, E Maros, A Marquina, S Marsat, F Martelli, I W Martin, R M Martin, D V Martynov, K Mason, E Massera, A Masserot, T J Massinger, M Masso-Reid, S Mastrogiovanni, A Matas, F Matichard, L Matone, N Mavalvala, N Mazumder, J J McCann, R McCarthy, D E McClelland, S McCormick, L McCuller, S C McGuire, J McIver, D J McManus, T McRae, S T McWilliams, D Meacher, G D Meadors, M Mehmet, A K Mehta, J Meidam, A Melatos, G Mendell, R A Mercer, L Mereni, E L Merilh, M Merzougui, S Meshkov, C Messenger, C Messick, R Metzdorff, P M Meyers, H Miao, C Michel, H Middleton, E E Mikhailov, L Milano, A L Miller, A Miller, M Millhouse, J C Mills, M C Milovich-Goff, O Minazzoli, Y Minenkov, A Mishkin, C Mishra, T Mistry, S Mitra, V P Mitrofanov, G Mitselmakher, R Mittleman, G Mo, D Moffa, K Mogushi, S R P Mohapatra, M Montani, C J Moore, D Moraru, G Moreno, S Morisaki, B Mours, C M Mow-Lowry, Arunava Mukherjee, D Mukherjee, S Mukherjee, N Mukund, A Mullavey, J Munch, E A Muñiz, M Muratore, P G Murray, A Nagar, I Nardecchia, L Naticchioni, R K Nayak, J Neilson, G Nelemans, T J N Nelson, M Nery, A Neunzert, K Y Ng, S Ng, P Nguyen, D Nichols, S Nissanke, F Nocera, C North, L K Nuttall, M Obergaulinger, J Oberling, B D O'Brien, G D O'Dea, G H Ogin, J J Oh, S H Oh, F Ohme, H Ohta, M A Okada, M Oliver, P Oppermann, Richard J Oram, B O'Reilly, R G Ormiston, L F Ortega, R O'Shaughnessy, S Ossokine, D J Ottaway, H Overmier, B J Owen, A E Pace, G Pagano, M A Page, A Pai, S A Pai, J R Palamos, O Palashov, C Palomba, A Pal-Singh, Huang-Wei Pan, B Pang, P T H Pang, C Pankow, F Pannarale, B C Pant, F Paoletti, A Paoli, A Parida, W Parker, D Pascucci, A Pasqualetti, R Passaquieti, D Passuello, M Patil, B Patricelli, B L Pearlstone, C Pedersen, M Pedraza, R Pedurand, A Pele, S Penn, C J Perez, A Perreca, H P Pfeiffer, M Phelps, K S Phukon, O J Piccinni, M Pichot, F Piergiovanni, G Pillant, L Pinard, M Pirello, M Pitkin, R Poggiani, D Y T Pong, S Ponrathnam, P Popolizio, E K Porter, J Powell, A K Prajapati, J Prasad, K Prasai, R Prasanna, G Pratten, T Prestegard, S Privitera, G A Prodi, L G Prokhorov, O Puncken, M Punturo, P Puppo, M Pürrer, H Qi, V Quetschke, P J Quinonez, E A Quintero, R Quitzow-James, F J Raab, H Radkins, N Radulescu, P Raffai, S Raja, C Rajan, B Rajbhandari, M Rakhmanov, K E Ramirez, A Ramos-Buades, Javed Rana, K Rao, P Rapagnani, V Raymond, M Razzano, J Read, T Regimbau, L Rei, S Reid, D H Reitze, W Ren, F Ricci, C J Richardson, J W Richardson, P M Ricker, K Riles, M Rizzo, N A Robertson, R Robie, F Robinet, A Rocchi, L Rolland, J G Rollins, V J Roma, M Romanelli, R Romano, C L Romel, J H Romie, K Rose, D Rosińska, S G Rosofsky, M P Ross, S Rowan, A Rüdiger, P Ruggi, G Rutins, K Ryan, S Sachdev, T Sadecki, M Sakellariadou, L Salconi, M Saleem, A Samajdar, L Sammut, E J Sanchez, L E Sanchez, N Sanchis-Gual, V Sandberg, J R Sanders, K A Santiago, N Sarin, B Sassolas, B S Sathyaprakash, P R Saulson, O Sauter, R L Savage, P Schale, M Scheel, J Scheuer, P Schmidt, R Schnabel, R M S Schofield, A Schönbeck, E Schreiber, B W Schulte, B F Schutz, S G Schwalbe, J Scott, S M Scott, E Seidel, D Sellers, A S Sengupta, N Sennett, D Sentenac, V Sequino, A Sergeev, Y Setyawati, D A Shaddock, T Shaffer, M S Shahriar, M B Shaner, L Shao, P Sharma, P Shawhan, H Shen, R Shink, D H Shoemaker, D M Shoemaker, S Shyam-Sundar, K Siellez, M Sieniawska, D Sigg, A D Silva, L P Singer, N Singh, A Singhal, A M Sintes, S Sitmukhambetov, V Skliris, B J J Slagmolen, T J Slaven-Blair, J R Smith, R J E Smith, S Somala, E J Son, B Sorazu, F Sorrentino, T Souradeep, E Sowell, A P Spencer, A K Srivastava, V Srivastava, K Staats, C Stachie, M Standke, D A Steer, M Steinke, J Steinlechner, S Steinlechner, D Steinmeyer, S P Stevenson, D Stocks, R Stone, D J Stops, K A Strain, G Stratta, S E Strigin, A Strunk, R Sturani, A L Stuver, V Sudhir, T Z Summerscales, L Sun, S Sunil, J Suresh, P J Sutton, B L Swinkels, M J Szczepańczyk, M Tacca, S C Tait, C Talbot, D Talukder, D B Tanner, M Tápai, A Taracchini, J D Tasson, R Taylor, F Thies, M Thomas, P Thomas, S R Thondapu, K A Thorne, E Thrane, Shubhanshu Tiwari, Srishti Tiwari, V Tiwari, K Toland, M Tonelli, Z Tornasi, A Torres-Forné, C I Torrie, D Töyrä, F Travasso, G Traylor, M C Tringali, A Trovato, L Trozzo, R Trudeau, K W Tsang, M Tse, R Tso, L Tsukada, D Tsuna, D Tuyenbayev, K Ueno, D Ugolini, C S Unnikrishnan, A L Urban, S A Usman, H Vahlbruch, G Vajente, G Valdes, N Van Bakel, M Van Beuzekom, J F J Van Den Brand, C Van Den Broeck, D C Vander-Hyde, J V Van Heijningen, L Van Der Schaaf, A A Van Veggel, M Vardaro, V Varma, S Vass, M Vasúth, A Vecchio, G Vedovato, J Veitch, P J Veitch, K Venkateswara, G Venugopalan, D Verkindt, F Vetrano, A Viceré, A D Viets, D J Vine, J-Y Vinet, S Vitale, T Vo, H Vocca, C Vorvick, S P Vyatchanin, A R Wade, L E Wade, M Wade, R Walet, M Walker, L Wallace, S Walsh, G Wang, H Wang, J Z Wang, W H Wang, Y F Wang, R L Ward, Z A Warden, J Warner, M Was, J Watchi, B Weaver, L-W Wei, M Weinert, A J Weinstein, R Weiss, F Wellmann, L Wen, E K Wessel, P Weßels, J W Westhouse, K Wette, J T Whelan, B F Whiting, C Whittle, D M Wilken, D Williams, A R Williamson, J L Willis, B Willke, M H Wimmer, W Winkler, C C Wipf, H Wittel, G Woan, J Woehler, J K Wofford, J Worden, J L Wright, D S Wu, D M Wysocki, L Xiao, H Yamamoto, C C Yancey, L Yang, M J Yap, M Yazback, D W Yeeles, Hang Yu, Haocun Yu, S H R Yuen, M Yvert, A K Zadrożny, M Zanolin, T Zelenova, J-P Zendri, M Zevin, J Zhang, L Zhang, T Zhang, C Zhao, M Zhou, Z Zhou, X J Zhu, M E Zucker, and J Zweizig. A guide to LIGO–Virgo detector noise and extraction of transient gravitational-wave signals. *Classical and Quantum Gravity*, 37(5):055002, March 2020.

[2] Teviet Creighton. Gravitational waves demystified.

[3] T. Damour, A. Nagar, and M. Trias. Accuracy and effectualness of closed-form, frequency-domain waveforms for non-spinning black hole binaries. *Physical Review D*, 83(2):024006, January 2011. arXiv:1009.5998 [gr-qc].

[4] Jaynes E. T. and Bretthorst G. Larry. *Probability Theory : The Logic of Science.* Cambridge University Press, 2003.

[5] Frank Ohme. Analytical meets numerical relativity: status of complete gravitational waveform models for binary black holes. *Classical and Quantum Gravity*, 29(12):124002, June 2012.

[6] Michael Pürrer, Mark Hannam, and Frank Ohme. Can we measure individual black-hole spins from gravitational-wave observations? *Physical Review D*, 93(8):084042, April 2016. arXiv:1512.04955 [astro-ph, physics:gr-qc].